



# Land surface temperature relation with normalized satellite indices for the estimation of spatio-temporal trends in temperature among various land use land cover classes of an arid Potohar region using Landsat data

Aqil Tariq<sup>1</sup> · Iqra Riaz<sup>2,3</sup> · Zulfiqar Ahmad<sup>4</sup> · Bisheng Yang<sup>1</sup> · Muhammad Amin<sup>2</sup> · Rukhsana Kausar<sup>3</sup> · Shaista Andleeb<sup>5</sup> · Muhammad Aslam Farooqi<sup>6</sup> · Muhammad Rafiq<sup>7</sup>

Received: 24 July 2018 / Accepted: 2 December 2019 / Published online: 26 December 2019  
© Springer-Verlag GmbH Germany, part of Springer Nature 2019

## Abstract

In terrestrial landscape architecture, land surface temperature (LST) is a key estimator of local climate, vegetation growth, and urban transition. It also represents the environmental factors that influence the land cover patterns using temperature variation over land use land cover (LULC) classes. In the present study, various geospatial techniques have been implemented to analyze the spatio-temporal trends in temperature among different LULC of an arid Potohar region of Pakistan using Landsat 7 (ETM+) and 8 (OLI & TIRS) and the relationship between different normalized satellite indices and LST. Results of the seasonal fluctuation in winter showed temperature range of 0–57, 0–50, 04–31 and 7–39 °C for the year 2000, 2005, 2010, and 2015, respectively, while the summer exhibited the temperature range of 24–48, 27–57, 22–48, and 12–41 °C for the year 2000, 2005, 2010, and 2015, respectively. The analysis established a direct correlation between LST and normalized difference vegetation index and normalized difference water index, and an indirect correlation among LST and normalized difference soil index, normalized difference built-up index and built-up index. The findings are critically important for planning and development division for sustainable use of land resources for urbanization extension projects. Future research will highlight the change in the area occupied by different land featured classes and their impacts on LST over a specified period.

**Keywords** LST · LULC · Landsat · GIS indices · Remote sensing

---

Aqil Tariq, Iqra Riaz, Zulfiqar Ahmad, Bisheng Yang, Muhammad Amin, Rukhsana Kausar, Shaista Andleeb, Muhammad Aslam Farooqi and Muhammad Rafiq have contributed equally to this work.

---

**Electronic supplementary material** The online version of this article (<https://doi.org/10.1007/s12665-019-8766-2>) contains supplementary material, which is available to authorized users.

---

✉ Zulfiqar Ahmad  
zulfiqar@whu.edu.cn; imzulfiqarahmad@gmail.com

<sup>1</sup> State Key Laboratory of Information Engineering in Surveying, Mapping and Remote Sensing, Wuhan University, Hubei 430079, China

<sup>2</sup> Institute of Geo-information and Earth Observation (IGEO), PMAS Arid Agriculture University, Rawalpindi 46300, Pakistan

<sup>3</sup> Department of Environmental Science, International Islamic University Islamabad, Islamabad 44000, Pakistan

## Introduction

Land surface temperature is the fundamental climatic parameter in determining the surface radiation and the energy exchange (He et al. 2019). It is also essential for determining the dynamics of the earth's surface, which impact-feedback loops that occur over a wide range of temporal and spatial

<sup>4</sup> State Key Laboratory of Water Resources and Water Hydropower Engineering Science, Wuhan University, Wuhan 430072, Hubei, China

<sup>5</sup> Department of Wildlife Management and Environmental Sciences, Pir Mehr Ali Shah-Arid Agriculture University, Rawalpindi, Pakistan

<sup>6</sup> Department of Entomology, UCA & ES, The Islamia University of Bahawalpur, Bahawalpur 63100, Pakistan

<sup>7</sup> Department of Computer Science, Federal Urdu University of Arts, Science and Technology, Islamabad 44000, Pakistan

scales (Simó et al. 2019). Among these parameters, land use/land cover (LU/LC) and land surface temperature (LST) are the most important. The concept of LST has been widely used by many researchers across the globe for unpredictable rainfall, temperature fluctuations, vegetation patterns, and urban area agglomeration are aspects that alter/shift the land use/land cover in a region (Owojori and Hongjie 2015). The shifting of this land use/land cover is attributed to anthropogenic activities that alter the physical characteristics of the land surface and abrupt changes in temperature in a particular region (Srivanit et al. 2012). It is well documented that as land surface cover changes, the surface temperature of that particular area also changes (Buyadi et al. 2013; Hua and Ping 2018). Hence, measurement of land surface temperature and its variation over a specified period significantly depicts the variation in land use/land cover of that local region.

Previously, different techniques have been employed for the measurement of land surface temperature through ground base data, but that is costly and cumbersome (Rehman et al. 2015). Dense time-series observations (DTSO) frequently employed in monitoring approaches related to the remote sensing (RS) and LST. The applicability of these DTSO in the assessment of the climate variability over a extended period can be improved by the integration of spatial data from multiple satellite systems (Kothe et al. 2019). The most valuable source of spatial information (30-m resolution) is Landsat images data (Lagüela et al. 2019). It not only helpful in continuous global coverage but also provide an opportunity to characterize human-scale processes (Chen et al. 2017). The operational Landsat 7 (ETM+) and Landsat 8 (OLI & TIRS) can provide a revisit frequency of 8 days at the equator (Chastain et al. 2019). The images obtained by Landsat sensors have a high spatial resolution for monitoring the urban thermal environment (Sobrino et al. 2012; Rongbo et al. 2007).

The Landsat 7 Enhanced Thematic Mapper Plus (ETM+) sensor is the successor of TM. However, on May 31st, 2003, the scan-line corrector (SLC) of ETM+ permanently failed, which caused roughly 22% of the pixels not to be scanned in any ETM+ images (referred to as SLC-off images) (Arvidson et al. 2006). For the generation of 16-day data in Landsat 7, a smooth and gap-filled time series data with 30 m spatial resolution were generated using Geo-statistical neighborhood method which involves scanned lines filling techniques. Additionally, it can also produce more accurate results than NSPI, specifically for the long time interval between the auxiliary input images and the target SLC-off images (Zhu et al. 2012). Therefore, the thermal infrared (TIR) remote sensing is a unique process for the estimation of land surface temperature at regional to global scale (Meng et al. 2017). Although, these approaches have been used widely to estimate the variations in land surface

temperature and their relationship with Land use/Land cover indices, yet estimation of LST and its variation over selected Land use/Land cover indices for an arid Potohar region using multi-spectral geospatial techniques has been merely studied (Cristóbal et al. 2009; Jiménez-Muñoz and Sobrino 2009; Mallick et al. 2008; Bala et al. 2019).

Therefore, the present study was planned to investigate the variation in temperature over wide range of classes and investigate relationship between normalized satellite indices including normalized difference vegetation index (NDVI), normalized difference water index (NDWI), normalized difference soil index (NDSI), normalized difference built-up index (NDBI), built-up index (BI) and LST. The arid Potohar region as study area due to its highly undulating topography and erratic rainfall pattern along with a wide variety of land covers like water bodies, barren land, built-up areas, and vegetated land. To the best of our knowledge, this is the first report on estimation of LST and its variation over Land use/Land cover indices for an arid Potohar region of Pakistan using Landsat-7 (ETM+) and 8 (OLI + TIRS) imagery with two valuable thermal bands Band 6 (ETM+) and Band 10 (OLI + TIRS).

## Study area

The arid Potohar region (32.5° N to 34.0° N Latitude and 72° E to 74° E Longitude) was selected as a study area. The geographic location of the study area has been shown in Fig. 1. The region comprises four districts, namely Attock, Jhelum, Rawalpindi, and Chakwal, covering an area of 28,488.9 km<sup>2</sup> (Rashid and Rasul 2007). The terrain of the region was undulating, and the average height of the mountain was 450–900 m (3000 ft), which extend up to 72 km. The general methodology adopted for this study has been summarized in the flow chart diagram (Fig. 2).

## Materials and methods

### Data collection and processing

LST and Normalized satellite indices were calculated using Matlab 2015 and Erdas 2016. The shapefiles of respective areas were created, and area of interest (AOI) was extracted using Erdas 2016 (Supplementary Table 3). The next step involved was downloading satellite data (cloud cover 0%) of Landsat-7 & 8 were used of arid Potohar region for this study. The four-year imaging (five-year interval 2000, 2005, 2010, and 2015) were downloaded from USGS Earth Explorer website (<https://www.usgs.gov/>) (day, level-1G product) and referenced to the Universal Transverse Mercator (UTM) Projection System (Table 1). Landsat 7 images

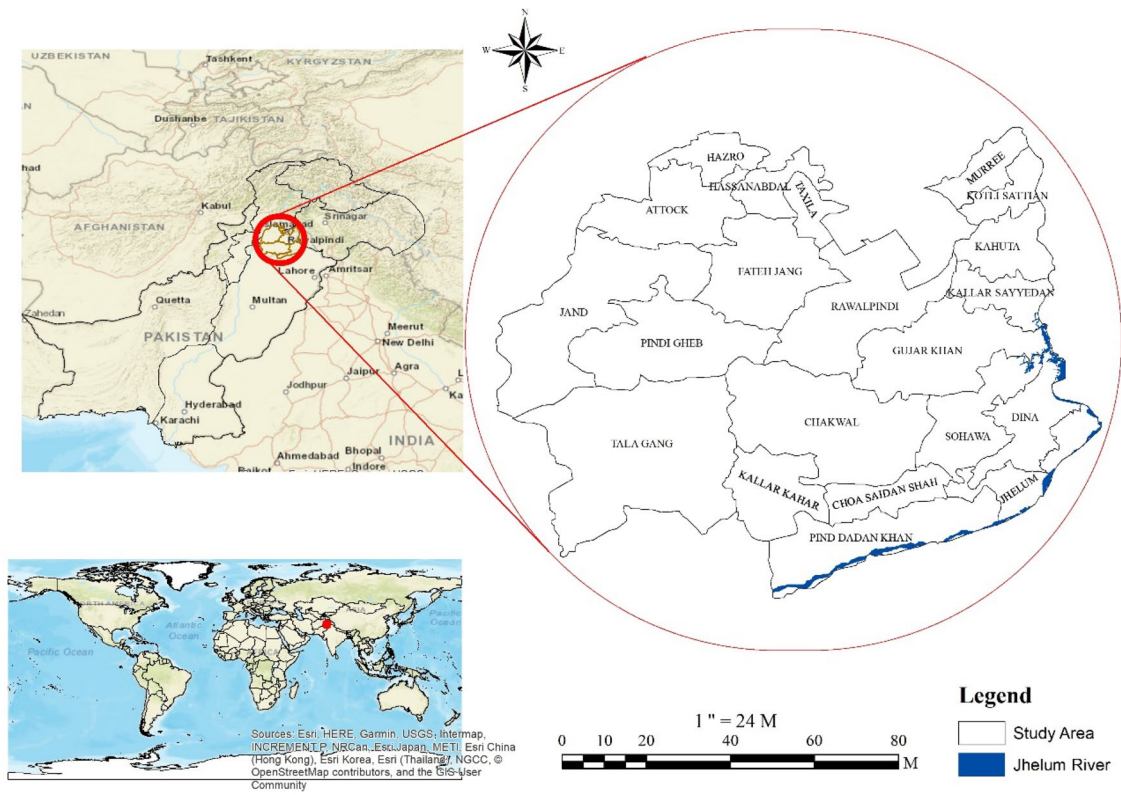


Fig. 1 Location map of study area (Potohar Region showing District Rawalpindi, Chakwal, Attock and Jhelum)

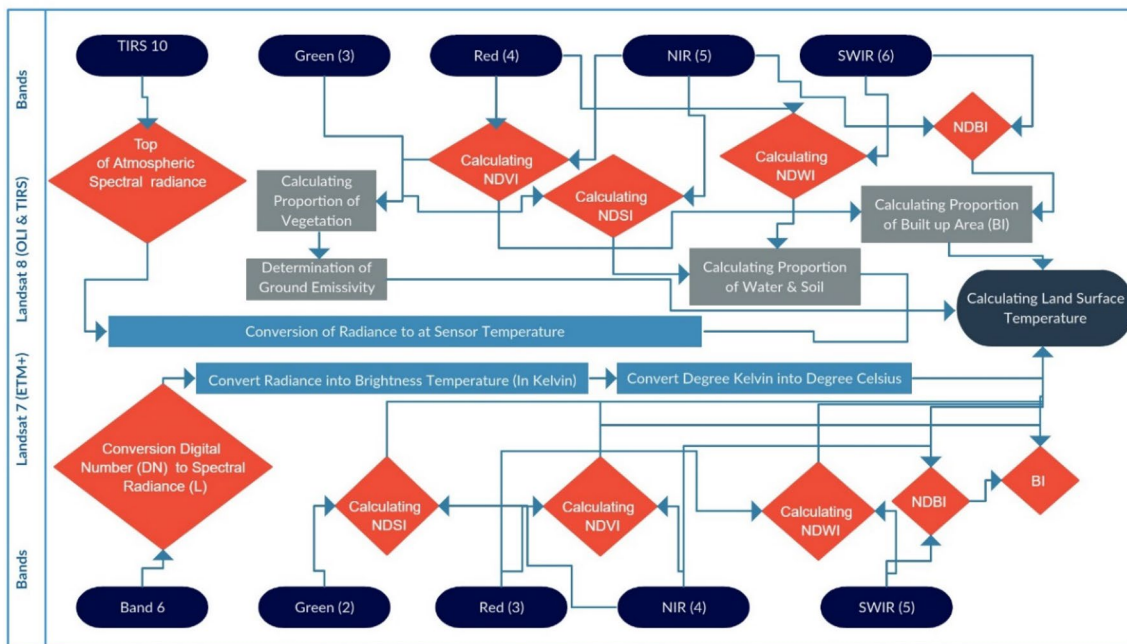


Fig. 2 Flow chart of general methodology

**Table 1** Data collection

S. no	Season	Dated	Mosaic						
			Row	Path	Row	Path	Row	Path	
01	Winter	2000	150	37	150	36	151	37	Landsat 7 (ETM)
02	Summer	2000	150	37	150	36	151	37	
03	Winter	2005	150	37	150	36	151	37	
04	Summer	2005	150	37	150	36	151	37	
05	Winter	2010	150	37	150	36	151	37	
06	Summer	2010	150	37	150	36	151	37	
07	Winter	2015	150	37	150	36	151	37	Landsat 8 (OLI)
08	Summer	2015	150	37	150	36	151	37	

with 08 bands (of which the band 6 was thermal band), and ETM+ bands (1–5 and 7 bands) of 30 m spatial resolution, were used to estimate Land use/Land cover (LULC) map of the study area. The spatial resolution of thermal bands was 60 m, which was re-sampled to 30 m for distribution according to the method as described by Jimenez-Munoz et al. (2014). Landsat 8 images with 11 bands (of which band 10 and 11 were thermal, 1–7 & 9 were OLI, band 8 was panchromatic, and band 10 and 11 were thermal) were used to estimate Land use/Land cover (LULC) map (Table 2). The Landsat 8 images had 30 m spatial, 12 bit radiometric, and 16 days temporal resolution. The spatial resolution of thermal bands was 100 m, which was re-sampled to 30 m for distribution (Supplementary Table 1) according to the method as described by Jimenez-Munoz et al. (2014).

### Image pre-processing

For removal of strips and gaps during downloading of LANDSAT ETM+ data, Environment for Visualizing Images (ENVI) software was used. For extraction of data of

interest in the present study, Layer stack and create image, and the mosaic of all images tools was used. Similarly, removal of haze from all layers during the downloading of LANDSAT8 (OLI & TIRS) was done using these tools (Supplementary Table 3).

### Land cover indices determination

The land cover indices (NDVI, NDWI, NDSI, NDBI, and BI) used in this study, and were obtained from visible portion (VP) Green (G), Red (R), Near Infrared (NIR) and Short Wave Infra-Red (SWIR) reflectance bands which were extracted from the LANDSAT 7 (ETM+) and LANDSAT 8 (OLI & TIRS) images (Xu et al. 2013). The estimation of vegetation cover, water bodies, built-up area, and barren land, was carried out according to the procedure as described by Smakhtin and Hughes (2007). The various land cover index maps were obtained using the method as described by Weng (2004). Data regarding the calculation of various indices have been shown in Supplementary Table 2.

**Table 2** Description of Landsat7 (ETM+) and Landsat 8 (OLI & TIRS)

S. no	Landsat 7 (ETM+)			Bands	Landsat 8 (OLI & TIRS)		
	Resolution (m)	Wavelength (Micrometer)	Band Name		Band Name	Wavelength (Micrometers)	Resolution (m)
1	30	0.45–0.52	Blue	Ultra Blue (coastal/aerosol)	0.435–0.451	30	
2	30	0.52–0.60	Green	Blue	0.452–0.512	30	
3	30	0.63–0.69	Red	Green	0.533–0.590	30	
4	30	0.77–0.90	NIR	Red	0.636–0.673	30	
5	30	1.55–1.75	SWIR1	NIR	0.851–0.879	30	
6	60*(30)	10.40–12.50	Thermal	SWIR1	1.566–1.651	30	
7	30	2.09–2.35	SWIR2	SWIR2	2.107–2.294	30	
8	15	0.52–0.90	Panchromatic	Panchromatic	0.503–0.676	15	
9				Cirrus	1.363–1.384	30	
10				TIRS1	10.60–11.19	100*(30)	
11				TIRS2	11.50–12.51	100*(30)	

### Image classification

To investigate the changes occurring at the regional scale, the land cover classification was carried out to develop the LULC maps of arid Potohar region for the year 2000, 2005, 2010 and 2015. Categories used for classification were built-up area, water bodies, vegetation area, and barren land. A supervised signature extraction with the maximum likelihood algorithm was employed to classify the Landsat images. Both statistical and geospatial analysis of feature selection was used to find out the most active band in discrimination of each category and classification. The description of each normalized satellite index has been given in Supplementary Table 2.

### Extraction of land surface temperature from Landsat 7(ETM+)

The LST from Landsat 7 dataset was retrieved according to the procedure as described by Chander et al. (2009). Briefly, the radiance values derived were used to calculate at satellite brightness temperature (i.e., black body temperature) followed by a correction for spectral emissivity according to the nature of the landscape (Weng et al. 2004). LST maps with band 6 (Landsat-7), band 10 (Landsat 8) and top of atmosphere brightness temperature values have been expressed in Kelvin for each of the study areas.

### Conversion of the digital number (DN) to spectral radiance (Lλ)

The Spectral Radiance was calculated as:

$$L\lambda = \text{Grescale} \times \text{QCAL} + \text{Brescale} \tag{1}$$

which is also expressed as

$$L\lambda = \frac{(\text{LMAX } \lambda - \text{LMIN } \lambda)}{(\text{QCALMAX} - \text{QCALMIN})}(\text{QCAL} - \text{QCALMIN}) + \text{LMIN } \lambda \tag{2}$$

where  $L\lambda$  is the Spectral Radiance at the sensors aperture in  $\left[\frac{W}{m^2} \times \text{ster} \times \mu\text{m}\right]$ , QCAL is the quantized calibrated pixel value in DN (Digital Number), LMIN  $\lambda$  is the spectral radiance that is scaled to QCALMIN in  $\left[\frac{W}{m^2} \times \text{ster} \times \mu\text{m}\right]$ , LMAX  $\lambda$  is the spectral radiance that is scaled to QCALMAX in  $\left[\frac{W}{m^2} \times \text{ster} \times \mu\text{m}\right]$ , QCALMIN is the minimum quantized calibrated pixel value (corresponding to LMIN  $\lambda$ ) in DN, QCALMAX=the maximum quantized calibrated pixel value (corresponding to LMAX  $\lambda$ ) in DN (255).

### Conversion of spectral radiance (Lλ) to At-satellite brightness temperatures (TB) Corrections

The conversion of spectral radiance to temperature ( $k$ ) was done according to the following equation

$$T_B = \frac{K_2}{L_n \left( \frac{K_1}{L_\lambda} + 1 \right)} \tag{3}$$

where  $T_B$ =At-satellite brightness temperature (K),  $K_2$ =calibration constant 2 calculated from Table 3,  $K_1$ =Calibration constant 1 calculated from Table 3,  $L_\lambda$ =spectral radiance in  $\left[\frac{W}{m^2} \times \text{ster} \times \mu\text{m}\right]$ .

### Conversion of brightness temperatures (K) corrections to brightness temperatures (°C) corrections

$T_B$  = surface temperature (°C)

$$T_B = T_B - 273.15 \tag{4}$$

### Extraction of land surface temperature from Landsat 8 (OLI & TIRS)

For absolute temperature recovery, the digital number (DN) of the thermal infrared band was converted to spectral radiance ( $L_\lambda$ ) using the Eq. (5) as stated by Rosas et al. (2017).

$$L_\lambda = M_L \times Q_{\text{cal}} + A_L \tag{5}$$

where,  $L_\lambda$ —top of atmospheric radiance  $\left[\frac{W}{m^2} \times \text{ster} \times \mu\text{m}\right]$ ,  $M_L$ —band-specific multiplicative rescaling factor from metadata 0.0003342 (radiance\_mult\_band\_X, where X is the band number),  $Q_{\text{cal}}$ —quantized and calibrated standard product pixel values of DN in the band 10 from image,  $A_L$ —band-specific additive rescaling factor from metadata 0.1 (radiance\_add\_band\_X, where X is the band number).

The radiance values obtained were used to estimate the brightness temperature of the satellite. The average brightness temperature of band 10 was calculated, and the surface temperature values of the region were analyzed at the time

**Table 3** Factors and their parameters

	Landsat 7 (ETM+)	Landsat 8 (OLI & TIRS)	Thermal Band Calibration Constants & Rescaling
	Constant 1-K1 Watts (m <sup>2</sup> *ster *μm)	Constant 2-K2 Kelvin (m <sup>2</sup> *ster *μm)	Rescaling
Landsat 7	666.09	1282.71	
Landsat 8	774.8853	1321.0789	M <sub>L</sub> 0.0003342 A <sub>L</sub> 0.10

of data recorded (Table 4). The conversion of Radiance to sensor temperature was done using equation as described by (Suresh et al. 2016).

$$T_B = \frac{K2}{\ln \left[ \left( \frac{K1}{L\lambda} \right) + 1 \right]} - 273.15 \tag{6}$$

where  $T_B$  = At-satellite brightness temperature (°C),  $K1$  and  $K2$  stand for the band-specific thermal conversion constant from the metadata,  $L\lambda$ —top of atmospheric spectral radiance.

For the Conversion of sensor temperature to temperature (celsius), the absolute zero value was added to radiant temperature (Table 3).

### Land surface temperature (LST) measurement

The absolute temperature or Land surface temperature (LST) was estimated from average brightness temperature acquired from band 10 & band 11, the wavelength of emitted radiance, land surface emissivity, and constant value  $P$ . Land surface emissivity was calculated from the vegetation fraction which, in turn, derived from NDVI value range. The absolute temperature was calculated according to the method as employed by (Latif and Kamsan 2017), while the Landsat visible and near-infrared bands were used for calculating the NDVI.

$$NDVI = \frac{NIR (band5) - R (band4)}{NIR (band5) + R (band4)} \tag{7}$$

where NIR represents the near-infrared band (Band5), and R represents the Red Band (Band4).

### Measurement of vegetation index, ground emissivity, and emissivity-corrected values

The vegetation index ( $P_v$ ) was calculated according to the equation as described by (Rong-bo et al. 2007)

$$P_v = \left( \frac{NDVI - NDVI_s}{NDVI_v - NDVI_s} \right)^2 \tag{8}$$

While the Ground Emissivity ( $\epsilon$ ) and Emissivity-corrected values were calculated according to the following equations (Pal and Ziaul 2017).

$$\epsilon = 0.004 \times P_v + 0.986 \tag{9}$$

The emissivity corrected land surface temperatures (LST) was computed as following (Artis and Carnahan 1982).

$$LST = \frac{T_B}{1} + W \left( \frac{T_B}{\rho} \right) \times \ln(\epsilon) \tag{10}$$

where LST = land surface temperature corrected;  $T_B$  = Brightness temperature ;  $w$  = Wavelength of emitted radiance (11.5  $\mu$ m) ;  $\epsilon$  = emissivity corrected and  $\rho$  is the density which can be represented as  $\rho = h c / \sigma = 1.438 \times 10^{-2} \text{ mk}$ .

Where  $\sigma$  is the Boltzmann constant ( $1.38 \times 10^{-23} \text{ J/K}$ ),  $h$  is Planck’s constant ( $6.626 \times 10^{-34} \text{ J s}$ ), and  $c$  is the velocity of light ( $2.998 \times 10^8 \text{ m/s}$ ).

To estimate the relationship between normalized satellite indices (NDVI, NDWI, NDSI, NDBI, and BI) and LST, approximately 100 randomly selected spot locations were taken for each LST and indices in ArcGIS. Point values were recorded, and regression analysis in SPSS was performed to quantify the LST relationship with extracted NDVI, NDWI, NDSI, NDBI, and BI.

## Results and discussion

### Land surface temperature change (LSTC)

The derivation of LST for arid Potohar region showed high spatio-temporal variability in land surface temperature. The maps are shown in Fig. 3 indicates that the winter temperature was in the range of 24–48, 0–50, 04–31, and 7–39 °C for the year 2000, 2005, 2010, and 2015, respectively. Murree, Kotli Sattian and Attock exhibited dense vegetation cover and were highlighted green as the region of reduced

**Table 4** Coefficient of determination for LST normalized satellite indices

	NDVI	NDWI	NDSI	NDBI	BI	LST
2000 winter	0.9309	0.8125	0.7337	0.7643	0.8084	0.9768
2000 summer	0.9782	0.9927	0.9637	0.9927	0.9637	0.8741
2005 winter	0.9796	0.8902	0.9846	0.929	0.9322	0.6307
2005 summer	0.997	0.9983	0.9955	0.9667	0.9796	0.8885
2010 winter	0.9309	0.8125	0.7643	0.7337	0.8084	0.9768
2010 summer	0.9566	0.9132	0.9242	0.9287	0.948	0.924
2015 winter	0.9972	0.9372	0.9594	0.9726	0.9897	0.8739
2015 summer	0.9906	0.951	0.9674	0.9875	0.9969	0.8675

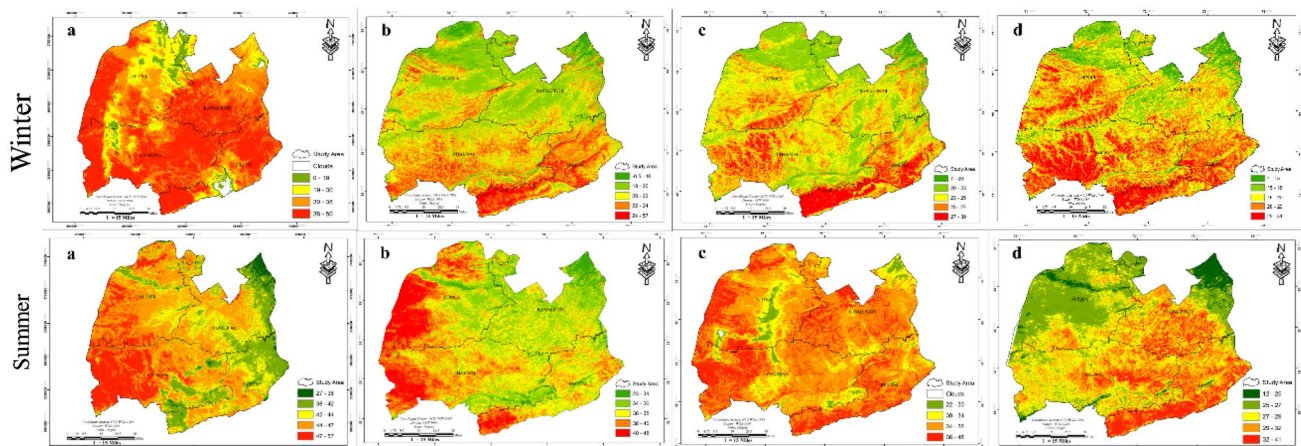


**Fig. 3** Land surface temperature (seasonal) of year **a** 2000, **b** 2005, **c** 2010 and **d** 2015

temperature, while Rawalpindi and Chakwal region were highlighted reddish as the regions of increased temperature. Result shown in Fig. 3 also indicates that the maximum temperature range (in winter) observed was 24–48, 0–50, 4–31, and 7–39 for the year 2000, 2005, 2010, and 2015, respectively. The maximum temperature range (in summer) observed was 0–57, 27–57, 22–48, and 12–41 for the year 2000, 2005, 2010 and 2015, respectively. The results were further validated by regression analysis, which also indicates that areas having water bodies and vegetation exhibited low surface temperature while built-up areas and barren land exhibited high surface temperature. Previous studies also illustrate the usefulness of Remotely sensed LST for radiant energy emitted from the ground surface, including Built-up areas, vegetation, bare ground, and water (Arnfield 2003; Voogt and Oke 2003).

### Land use and land cover mapping

Rainfed agriculture is the primary source of livelihood in the arid Potohar region. Rainfed areas are highly diverse, ranging from resource-rich areas to poor resource areas with much more restricted potential. Vegetation has a pronounced effect on climate change indicators such as temperature and precipitation patterns. Besides other factors, soil temperature and moisture, wind, relative humidity, and crop water requirements also affect the land use and land cover (Amir et al. 2019).

Results presented in Fig. 4 indicates the Land use land cover variations of arid Potohar region for the year 2000, 2005, 2010 and 2015. Figure 4a indicates the higher vegetation index, and low built-up area for the year 2000, while an increase in built-up area and low vegetation index for 2005. It might be because drought period prolongs during the year 2005 (Mallick et al. 2008). Similarly, a higher vegetation

index, built up area and moisture contents were observed for the year 2010. It was likely due to increased rainfall in that year (Ahmad et al. 2019). During the year 2015, the built-up area significantly increased due to the introduction of housing schemes in Rawalpindi and other cities in the year 2010–15 (Butt et al. 2015). Our results indicate that a significant enhancement in vegetation cover occurred in regions of Murree, Kotli Sattian, near Jhelum River, at Taxila and some areas of Chakwal district. The urban areas of Attock city, Chakwal, Rawalpindi, and Jhelum significantly increased due to residential and commercial development while water bodies and barren land found to be decreased in the year 2015 compared to the previous year.

### Relationship between land surface temperature (LST) and land use land cover classes (LULC)

The temperature variation was derived from two thermal bands; Thermal Band 6 (Landsat 7 ETM+) and TIR 10 (Landsat 8 OLI & TIRS) having the spatial resolution 30 m and swath width of 185 km (15° FOV from 705 km orbit). The appropriate color ramp symbology was selected to demonstrate the variation in temperature across the arid Potohar region for the studied years. 3 & 4 depict the projected LST maps over LULC maps of arid Potohar region. The variation in LST over various LULC might be due to the diverse nature of land use/cover type (Chaudhuri and Mishra 2016).

The Potohar plateau covers an area of about 5000 square miles (13,000 square km) and lies at an elevation of some 1200–1900 feet. The land resources of Potohar region characterized by fragmented land holdings. The contribution of agriculture activities in about 10 percent of total agricultural production (Adnan et al. 2009). In Fig. 5, the red spaces indicate the mean built-up areas where the average temperature was 25 °C and 40 °C in winter and summer,

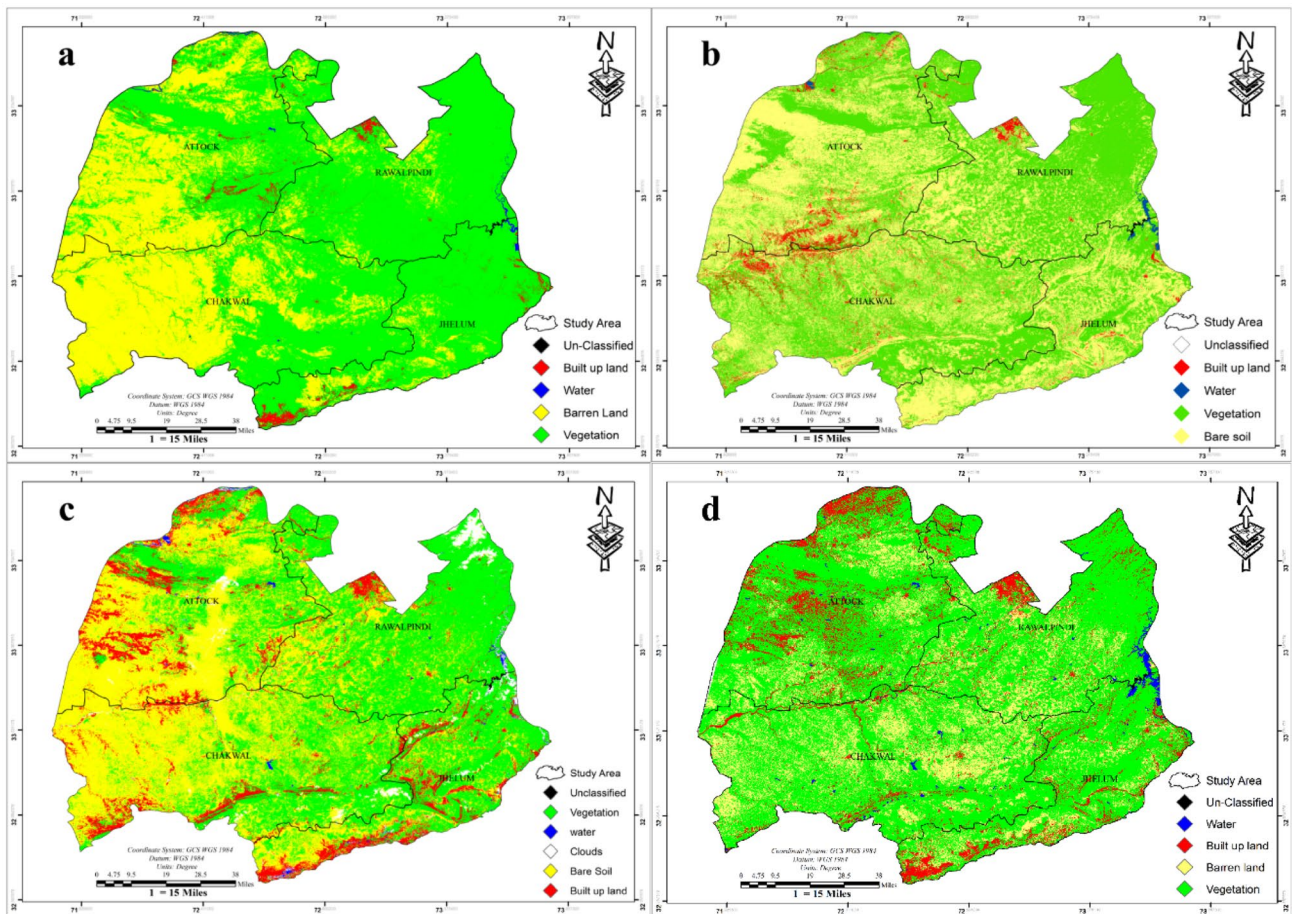


Fig. 4 Land cover classes of year a 2000, b 2005, c 2010 and d 2015

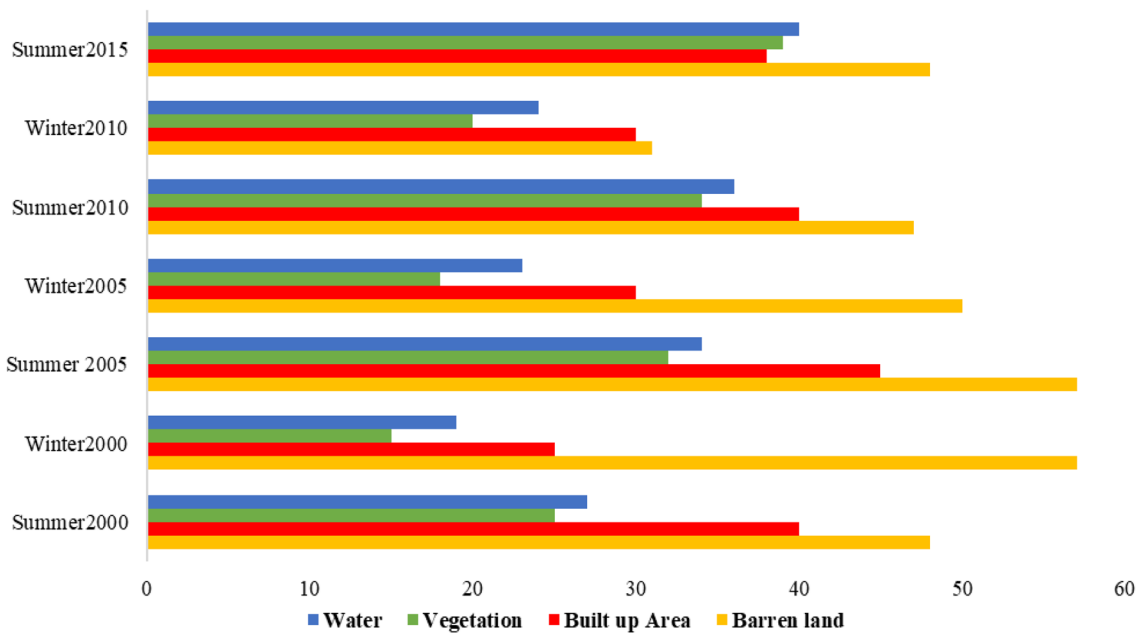


Fig. 5 LST trend change with LULC pattern



respectively, for the year 2000. The increase average temperature observed was 45 °C in summer and 30 °C in winter. The dry winter season observed might be due to lack of rainfall in the year 2000, which subsequently affected overall surface temperature (Jahangir et al. 2016). In 2010, the average temperature observed was 40 °C (in summer) and 30 °C (in winter), likely due to heavy rainfalls occurred in that year (Jahangir et al. 2016). During the year 2015, an increased in the built-up area was observed in Rawalpindi, Jhelum, Chakwal and Attock cities while a reduction in vegetation area and the temperature was observed in summer (38 °C) and winter (30 °C). It was likely due to the introduction of many housing societies and commercial development during the year 2015 in Rawalpindi district and surrounding areas. Our findings are also consistent with the findings of Xiong et al. (2012), who described that high-temperature anomalies are closely associated with built-up land, densely populated zones, and heavily industrialized districts. Similarly, in another study, it was analyzed that Landsat TM/ETM+ and Landsat 8 (OLI & TIRS) images NDVI and NDBI indices had a significantly close relationship (Rong-bo et al. 2007).

In Fig. 5, the yellow spaces indicate the barren areas shows an average temperature of 57 °C in summer and 48 °C in winter for the year 2000 while 57 °C in summer and 50 °C in winter for the year 2005. As discussed above, it might be due to the prolonged drought period in the year 2000, which resulted in increased surface temperature (Smakhtin and Hughes 2007). In 2010, due to the occurrence of heavy rainfall, the temperature in summer was 47 °C and 31 °C in winter. During the year 2015, the maximum average temperature observed in summer was 48 °C and 39 °C in winter. Low vegetation coverage is one of the main reasons for the LST effect (Weng and Yang 2004).

In Fig. 5, the greenish spaces indicate the vegetative areas exhibited a maximum average temperature of 25 °C in summer while 15 °C in winter for the year 2000. During the year 2005, a reduction in vegetation index was observed due to the drought period in arid Potohar region, and the average temperature observed in summer was 32 °C and 18 °C in winter. In 2010 the temperature in summer observed was 34 °C and 20 °C in winter. During the year 2015, the temperature in summer observed was 39 °C and 25 °C in winter due to the increase of built-up area and decrease of vegetation area in Potohar region (Peng et al. 2018).

In Fig. 5, The temperature of the water is usually lower than other kinds of land uses (Hathway and Sharples 2012; Peng et al. 2018) For bringing this relation more explicit, following (Yang et al. 2015). The water areas exhibited a maximum average temperature of 27 °C in summer and 19 °C in winter for the year 2000 which was increased up to 34 °C in summer and 23 °C in winter for the year 2005. In 2010, average temperature observed was 36 °C in summer and 24 °C in winter while during 2015, the average

temperature increased to 40 °C in summer and 29 °C in winter.

### LST relationship with normalized satellite indices

Based on the above observations in Figs. 3, 4 and 5, the ETM+ & OLI images from January 14, 2000 to August 20, 2015 were used to extract remote sensing information for the whole arid Potohar region, including the brightness temperature, Land use/land cover, NDVI, NDWI, NDSI, NDBI and BI (Figs. 6, 7, 8, 9 and 10).

Normalized difference vegetation index (NDVI) has been used to identify long-term variations in vegetation coverage (Fu and Burgher 2015). Land surface temperature changes are associated with vegetation cover/density (Xu et al. 2011). Extensive research has been conducted to find a real relationship between vegetation and surface temperature indexes (Kustas et al. 2003; Weng et al. 2004; Agam et al. 2007; Inamdar et al. 2008; Li et al. 2015). Figure 6a (winter, 2000) indicates NDVI values observed were from  $-0.640719$  to  $0.488889$  with the lowest temperature of 24 °C and the highest temperature of 48 °C. Results also revealed lower temperature high vegetative areas while the higher temperature in low vegetated areas. In Fig. 6b (winter, 2005) and Fig. 6c (winter, 2010), less vegetation could be observed during summer and winter because during that time drought period prevailed (Smakhtin and Hughes 2007). Figure 6d (winter, 2015) shows that NDVI values observed were from  $-0.343254$  to  $0.491024$  with the lowest and highest temperature of 7 °C and 39 °C. Results describe the high temperature in less dense vegetative areas, and low temperature in highly vegetated areas and vegetation move to the southern part in the study area. Results presented in Fig. 6a (summer, 2000), indicates that NDVI values observed were ranged from  $-0.482597$  to  $0.253333$  with the lowest temperature of 0 °C and the highest temperature of 57 °C for the year 2000. Figure 6b (summer, 2005) and in Fig. 6c (summer, 2010) summer was very harsh and dry with less vegetation (Smakhtin and Hughes 2007). In Fig. 6d (summer, 2015) the NDVI values observed were ranged from  $-0.362459$  to  $0.595055$  with the lowest temperature of 12 °C and the highest temperature of 41 °C. Results showed that the lowest temperature observed during winter was 0 °C, 39 °C for 2000 and 2015 while it was 24 °C for the same years during the summer season. Large vegetation areas in Murree and Jhelum exhibited high NDVI values while low vegetation in Attock and Chakwal district showed low NDVI values.

Surface water features depict the heat flow pattern and could be used to mitigate the urban heat island effects (Chang et al. 2007; Ahmed Memon et al. 2008; Bowler et al. 2010). Water bodies, have a little thermal response and are known to be efficient radiation absorbent (Gupta et al. 2019). Results presented in Fig. 7 indicates the NDWI spatial

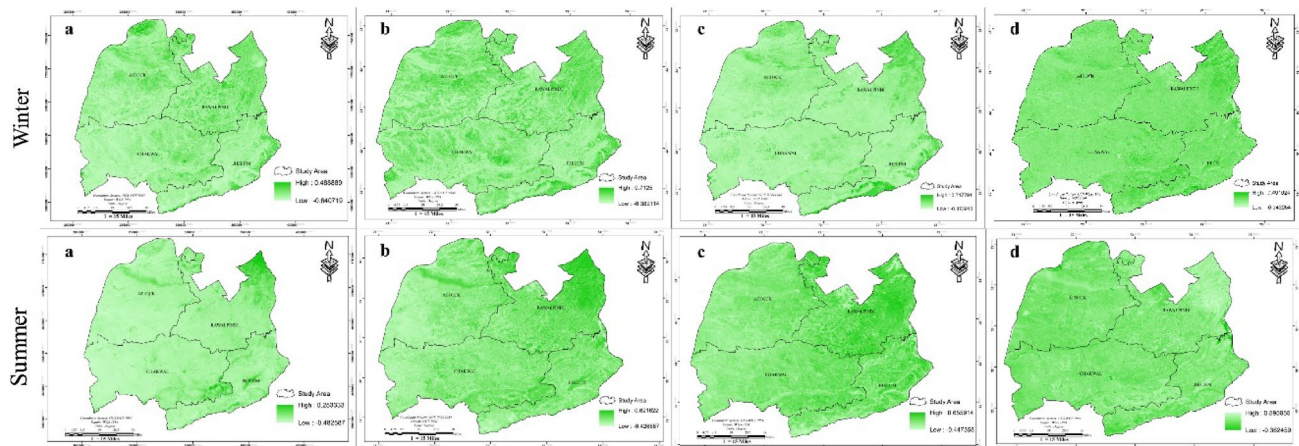


**Fig. 6** NDVI (seasonal) of year **a** 2000, **b** 2005, **c** 2010 and **d** 2015

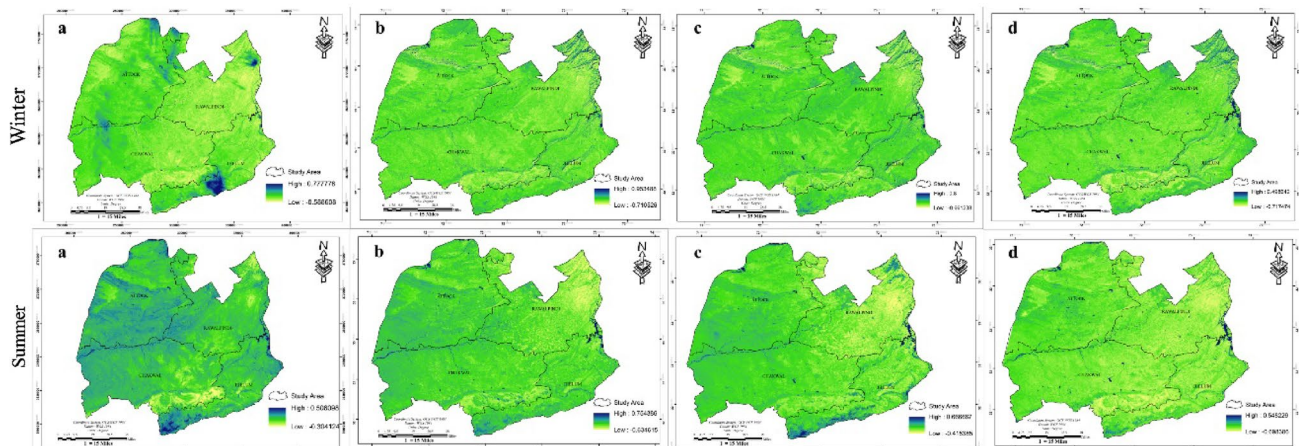


**Fig. 7** NDWI (seasonal) of year **a** 2000, **b** 2005, **c** 2010 and **d** 2015

distribution of water in Fig. 7a (winter, 2000), the NDWI values ranged were from 0.777778 to  $-0.588608$  with the lowest temperature of  $0\text{ }^{\circ}\text{C}$  and highest  $48\text{ }^{\circ}\text{C}$  temperature and Fig. 7b (winter, 2005),  $-0.710626$  to  $0.953488$  with the lowest temperature of  $0\text{ }^{\circ}\text{C}$  and highest  $50\text{ }^{\circ}\text{C}$ . In Fig. 7c (winter, 2010), the NDWI values ranged were from  $0.8$  to  $-0.661238$  with the lowest temperature of  $4\text{ }^{\circ}\text{C}$  and highest  $31\text{ }^{\circ}\text{C}$ . In Fig. 7d (winter, 2015), the NDWI values observed were ranged from  $-0.717474$  to  $0.499642$ , with the lowest and highest temperature of  $7\text{ }^{\circ}\text{C}$  and  $39\text{ }^{\circ}\text{C}$ , respectively.

Figure 7a (summer, 2000), the NDWI values ranged were from  $0.506098$  to  $-0.304124$  with the lowest temperature of  $0\text{ }^{\circ}\text{C}$  in summer and highest  $57\text{ }^{\circ}\text{C}$  and in Fig. 7b (summer, 2005),  $-0.634615$  to  $0.754386$  with the lowest temperature of  $27\text{ }^{\circ}\text{C}$  in summer and highest  $57\text{ }^{\circ}\text{C}$ . In Fig. 7c (summer, 2010), the NDWI values ranged were from  $0.666667$  to  $-0.415385$  with the lowest temperature of  $22\text{ }^{\circ}\text{C}$  in and highest  $48\text{ }^{\circ}\text{C}$ . In Fig. 7d (summer, 2015), the NDWI values

observed were ranged from  $-0.698386$  to  $0.548229$  with the lowest temperature of  $12\text{ }^{\circ}\text{C}$  in summer and highest  $41\text{ }^{\circ}\text{C}$ . Major water bodies of the district include River Jhelum and water coming from Tarbela Dam that passes with the boundary of Attock District (Ghoraba 2015).

Soil attributes directly influence the land surface temperature (Sayão et al. 2018). The soil spectral responses in the regions of visible (Vis), near-infrared (NIR), and short-wave infrared (SWIR) have a strong relationship with soil attributes with land surface temperature (Chang et al. 2001). Results presented in Fig. 8 indicates the NDSI values for the year 2000–15. Results indicate the NDSI values for the year 2000 (winter), were ranged from  $-0.382857$  to  $0.649123$  with the lowest and highest temperature of  $24$  and  $48\text{ }^{\circ}\text{C}$ , respectively (Fig. 8a). For the year 2005 (winter), the NDSI values observed were ranged from  $-0.633136$  to  $0.498992$  with the lowest temperature and the highest temperature of  $0$  and  $50\text{ }^{\circ}\text{C}$ , respectively (Fig. 8b). The NDSI values

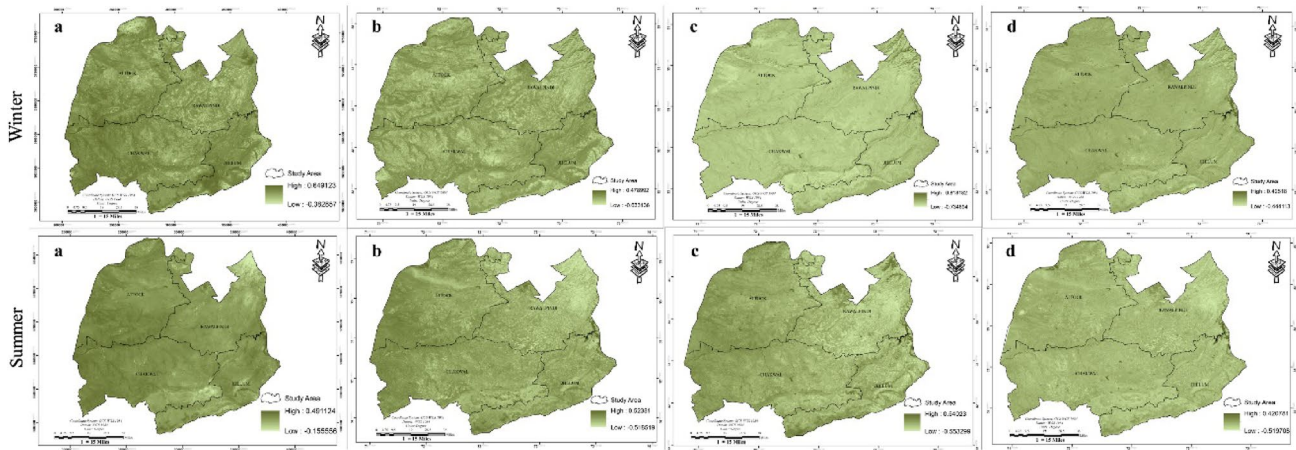


**Fig. 8** NDSI (winter) of year **a** 2000, **b** 2005, **c** 2010 and **d** 2015

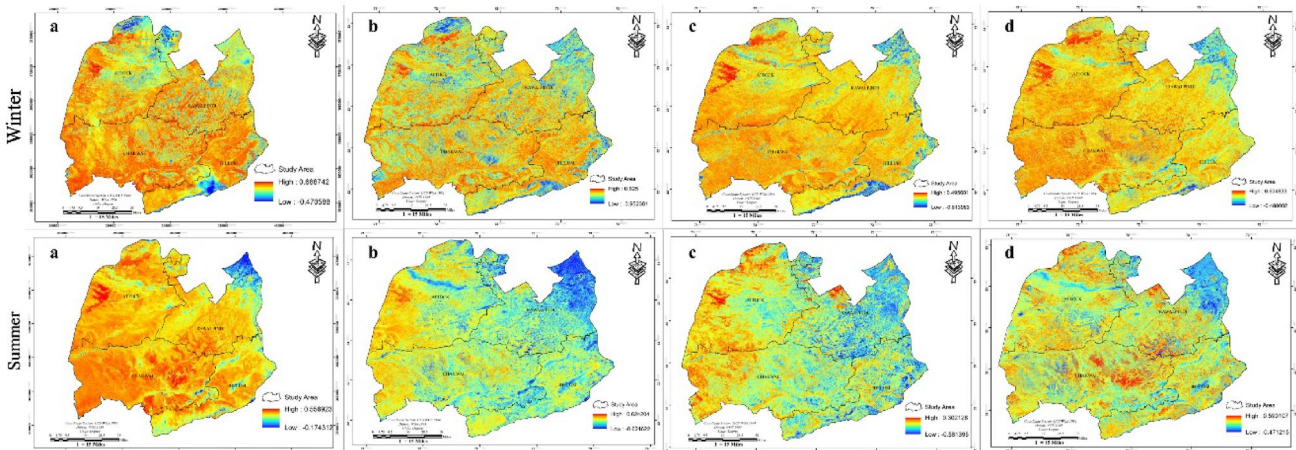


**Fig. 9** NDBI (seasonal) of year **a** 2000, **b** 2005, **c** 2010 and **d** 2015

for the year 2010 (winter) were ranged from  $-0.734894$  to  $0.818182$  with the lowest temperature and highest temperature of  $4$  and  $31$  °C, respectively. During the year 2015 (winter), the NDSI values observed were from  $-0.444113$  to  $0.42518$  with the lowest and highest temperature of  $7$  °C and  $39$  °C (Fig. 8d).

During the summer season, the NDSI values for the year 2000, ranged from  $-0.155556$  to  $0.491124$  with the lowest and highest temperature of  $48$  and  $57$  °C, respectively (Fig. 8a). For the year 2005, the NDSI values observed were ranged from  $-0.51851$  relationship between Land use/land cover to  $0.52381$  with the lowest and highest temperature of  $27$  and  $57$ °, respectively (Fig. 8b). In the year 2010, these NDSI values were ranged from  $-0.563299$  to  $0.54023$  with the lowest and highest temperature of  $22$  and  $48$  °C, respectively (Fig. 8c). During the year 2015, the NDSI values observed were from  $-0.519708$  to  $0.42087$

with the lowest and highest temperature of  $24$  and  $48$  °C, respectively (Fig. 8d).

The transformation of natural landscapes into human settlements has increased since urbanization starts, which has a considerable effect on built environments and global and local climates (Grimm et al. 2000). Cities are the primary areas for human activities and interactions, have faced extensive alterations in their land use and land cover (Li et al. 2011). Due to the intensity of urban development around the world, there is a growing body of studies attempting to investigate built-up index in various spatial and temporal scales (Jamei et al. 2019). Results of the present study indicate that during the year 2000 (winter) the NDBI values were ranged from  $-0.470588$  to  $0.688742$  with the lowest temperature and highest temperature of  $0$  and  $57$  °C (Fig. 9a). These values were from  $-0.621622$  to  $0.624204$  with the lowest temperature and highest temperature of  $0$  and  $50$  °C for the

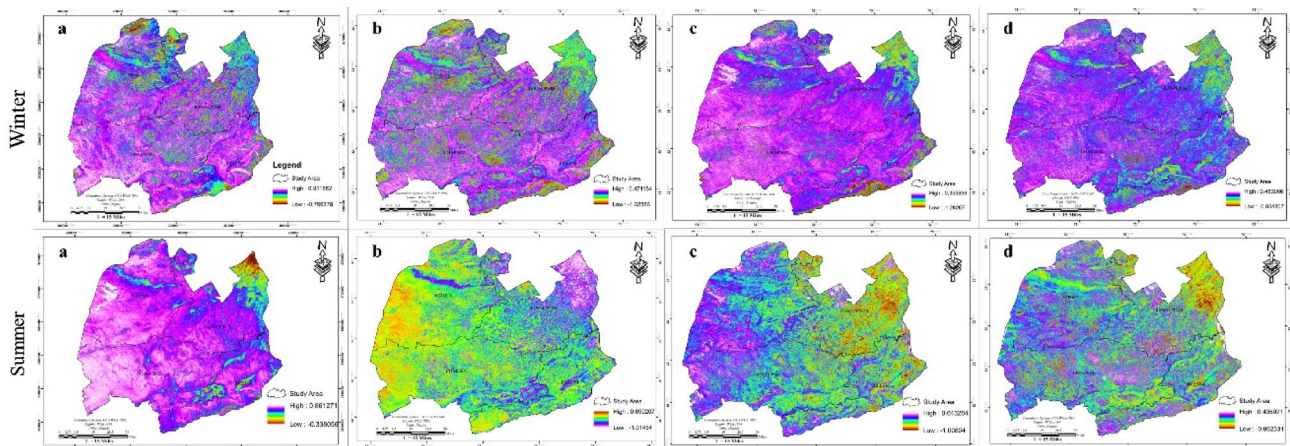


**Fig. 10** BI (seasonal) of year **a** 2000, **b** 2005, **c** 2010 and **d** 2015

year 2005 (winter) (Fig. 9b). Similarly, the NDBI values were from  $-0.952381$  to  $0.625$  with the lowest temperature and highest temperature of  $4$  and  $31$  °C for the year 2010 (winter) (Fig. 9c). The NDBI values observed were ranged from  $-0.488002$  to  $0.634833$  with the lowest temperature and highest temperature of  $7$  and  $39$  °C for the year 2015 (winter) (Fig. 9d). Similarly, For the year 2000 (summer), the NDBI values observed were ranged from  $-0.174312$  to  $0.556923$  with the lowest temperature and highest temperature of  $24$  and  $48$  °C (Fig. 9a). During the year 2005 (summer), the NDBI values were ranged from  $-0.621622$  to  $0.624204$  with the lowest temperature and highest temperature of  $27$  and  $57$  °C (Fig. 9b). In the year 2010 (summer), the NDBI values were ranged from  $-0.553299$  to  $0.54023$  with the lowest temperature and highest temperature of  $22$  and  $48$  °C (Fig. 9c). During the year 2015 (summer), the NDBI values were ranged from  $-0.581395$  to  $0.302128$  with the lowest temperature and highest temperature of  $12$  and  $41$  °C (Fig. 9d).

Urban indicators are for communicating relevant information to land planners (Handayani et al. 2018). Results are shown in Fig. 9a indicates BI values for the year 2000 (winter) observed were ranged from  $-0.483066$  to  $0.854801$  with the lowest and highest temperature of  $0$  and  $48$  °C, respectively. For the year 2005 (winter), these values were ranged from  $-1.28267$  to  $0.359896$  with the lowest temperature and highest temperature of  $0$  and  $50$  °C (Fig. 9b). In the year 2010 (winter), the BI values were ranged from  $-1.32386$  to  $0.471154$  with the lowest and highest temperature of  $4$  and  $31$  °C, respectively (Fig. 9c). During the year 2015 (winter), the BI values observed were ranged from  $-0.766378$  to  $0.911882$  with the lowest and highest temperature of  $7$  and  $39$  °C, respectively (Fig. 9d).

Similarly, for summer (2000), the BI values were ranged from  $-0.338056$  to  $0.861271$  with the lowest and highest

temperature of  $24$  and  $57$  °C, respectively (Fig. 9a). In 2005 (summer), these values were ranged from  $-1.01454$  to  $0.690207$  with the lowest and highest temperature of  $27$  and  $57$  °C, respectively (Fig. 9b). For summer, (2010), the BI values were ranged from  $-1.0084$  to  $0.643264$  with the lowest and highest temperature of  $22$  and  $48$  °C, respectively (Fig. 9c). During 2015 (summer), the BI values observed were ranged from  $-0.962331$  to  $0.405921$  with the lowest and highest temperature of  $12$  °C and  $41$  °C, respectively (Fig. 9d).

The relationship between Land use/land cover classes with derived land surface temperature shown in Figs. 7, 8, 9 and 10 indicates that there exists an inverse relationship between LST and water bodies, vegetation covers a direct relationship between built-up and barren land area.

### Measurement of the coefficient of determination for LST normalized satellite indices

Results presented in Table 4 indicates the seasonal and annual variability in LST with relation to different normalized satellite indices of arid Potohar region for the year 2000, 2005, 2010, and 2015. At seasonal and annual scales, the LST shows high interannual variability with NDVI, NDWI, NDSI, NDBI, and BI (Supplementary Fig. 1, 2, 3 and 4). At the annual scale (the year 2010 and 2015), a significant positive relationship observed among LST and NDSI and NDVI for the regions located in the western part of arid Potohar region while negative trends in the year 2000 and 2015 year. Whereas, an inverse relationship observed occurred in a minimal area (NDVI) of the eastern part, in which it is difficult to interpret LST trends.

At a seasonal scale, a significant relationship exists between LST and the different variables measured. Summer shows a generally positive trend (77.2%) between the

LST and indices measured. Nevertheless, negative trends were recorded in the areas of the Murree and upper part of Jhelum. These areas were characterized by high-density forest region, which results in a decrease in LST over the last half decades. For summer and winter, positive trends prevail over the southern and western part of the study area, likely due to lack of vegetation and low rainfall in that particular areas (Balouch et al. 2016).

## Conclusion

In this study, we systematically analyzed spatio-temporal trends in temperature in an arid Potohar region from 2000 to 2015 using multi-spectral remote sensing data. The study demonstrates the significance of land use/land cover in determining the surface heat balance that is the ultimate effect of temperature variation over the entire land cover area. An inverse relationship between LST and water bodies and vegetation cover was found while a direct relationship between LST and built up, and barren land area was observed. Hence, it is concluded that an increase in vegetative areas and water bodies can significantly reduce the overall surface temperature of any region due to the demonstrated inverse relation of NDVI and NDWI with LST. Use of RS & GIS techniques proves to be effective for the analysis of earth's surface variables like temperature, growth of vegetation, and built-up areas specifically in different geographical zones. Further research work will highlight the assessment of change in the area occupied by different land featured classes, i.e., dense forests, grasslands, built-up area and reserved forests and their impacts on Land surface temperature fluctuation concerning a specified period.

**Acknowledgments** Authors highly acknowledge Prof. Dr. David Crowley (Rtd.), Department of Environmental Sciences, University of California Riverside, USA, for taking a keen interest in proofreading and improving the quality of the manuscript. We dedicate this humble effort in honor of his services.

## Compliance with ethical standards

**Conflict of interest** There are no conflicts of interest.

## References

- Adnan S, Mahmood R, Khan AH (2009) Water balance conditions in rainfed areas of Potohar and Balochistan plateau during 1931–08. *World Appl Sci J* 7:162–169
- Agam N, Kustas WP, Anderson MC (2007) A vegetation index based technique for spatial sharpening of thermal imagery. *Remote Sens Environ* 107:545–558. <https://doi.org/10.1016/j.rse.2006.10.006>
- Ahmad S, Abbas G, Ahmed M (2019) Field Crops Research Climate warming and management impact on the change of phenology of the rice-wheat cropping system in Punjab, Pakistan. *Field Crops Res* 230:46–61. <https://doi.org/10.1016/j.fcr.2018.10.008>
- Ahmed Memon R, Leung DY, Chunho L (2008) A review on the generation, determination and mitigation of Urban Heat Island. *J Environ Sci* 20:120–128
- Amir S, Saqib Z, Khan A (2019) Land cover mapping and crop phenology of Potohar Region, Punjab, Pakistan. *Pak J Agric Sci* 56:187–196. <https://doi.org/10.21162/PAKJAS/19.7663>
- Artis DA, Carnahan WH (1982) Survey of emissivity variability in thermography of urban areas. *Remote Sens Environ* 12:313–329. [https://doi.org/10.1016/0034-4257\(82\)90043-8](https://doi.org/10.1016/0034-4257(82)90043-8)
- Arnfield AJ (2003) Two decades of urban climate research: a review of turbulence, exchanges of energy and water, and the urban heat island. *Int J Climatol* 23:1–26. <https://doi.org/10.1002/joc.859>
- Arvidson T, Goward S, Gasch J, Williams D (2006) Landsat-7 long-term acquisition plan: development and validation. *Photogramm Eng Remote Sens* 72:1137–1146
- Bala R, Prasad R, Yadav VP, Sharma J (2019) Spatial variation of urban heat island intensity in urban cities using modis satellite data. *Int Arch Photogramm Remote Sens Spat Inf Sci XLII-4/W16:147–151*. <https://doi.org/10.5194/isprs-archives-xlii-4-w16-147-2019>
- Balouch S, Rais M, Hussain I, Akram A (2016) Squamate diversity in different croplands of district Chakwal, Punjab, Pakistan. *J King Saud Univ Sci* 28:255–260. <https://doi.org/10.1016/j.jksus.2016.01.003>
- Bowler DE, Buyung-Ali L, Knight TM, Pullin AS (2010) Urban greening to cool towns and cities: a systematic review of the empirical evidence. *Landsc Urban Plan* 97:147–155. <https://doi.org/10.1016/j.landurbplan.2010.05.006>
- Butt A, Shabbir R, Ahmad SS, Aziz N (2015) Land use change mapping and analysis using remote sensing and GIS: a case study of Simly watershed, Islamabad, Pakistan. *Egypt J Remote Sens Space Sci* 18:251–259. <https://doi.org/10.1016/j.ejrs.2015.07.003>
- Buyadi SNA, Mohd WMNW, Misni A (2013) Green spaces growth impact on the urban microclimate. *Procedia Soc Behav Sci* 105:547–557. <https://doi.org/10.1016/j.sbspro.2013.11.058>
- Chander G, Markham BL, Helder DL, Ali E (2009) Remote Sensing of Environment Summary of current radiometric calibration coefficients for Landsat MSS, TM, ETM+, and EO-1 ALI sensors. *Remote Sens Environ* 113:893–903. <https://doi.org/10.1016/j.rse.2009.01.007>
- Chang C-W, Laird DA, Mausbach MJ, Hurburgh CR (2001) Near-infrared reflectance spectroscopy-principal components regression analyses of soil properties. *Soil Sci Soc Am J* 65:480. <https://doi.org/10.2136/sssaj2001.652480x>
- Chang CR, Li MH, Chang SD (2007) A preliminary study on the local cool-island intensity of Taipei city parks. *Landsc Urban Plan* 80:386–395. <https://doi.org/10.1016/j.landurbplan.2006.09.005>
- Chastain R, Housman I, Goldstein J (2019) Remote sensing of environment empirical cross sensor comparison of sentinel-2A and 2B MSI, Landsat-8 OLI, and Landsat-7 ETM+ top of atmosphere spectral characteristics over the conterminous United States. *Remote Sens Environ* 221:274–285. <https://doi.org/10.1016/j.rse.2018.11.012>
- Chaudhuri G, Mishra NB (2016) Spatio-temporal dynamics of land cover and land surface temperature in Ganges-Brahmaputra delta: a comparative analysis between India and Bangladesh. *Appl Geogr* 68:68–83. <https://doi.org/10.1016/j.apgeog.2016.01.002>
- Chen F, Yang S, Yin K, Chan P (2017) Science direct challenges to quantitative applications of Landsat observations for the urban thermal environment. *J Environ Sci* 59:80–88. <https://doi.org/10.1016/j.jes.2017.02.009>
- Cristóbal J, Jiménez-Muñoz JC, Sobrino JA, Ninyerola M, Pons X (2009) Improvements in land surface temperature retrieval from the Landsat series thermal band using water vapor and

- air temperature. *J Geophys Res* 114:D08103. <https://doi.org/10.1029/2008JD010616>
- Fu B, Burgher I (2015) Riparian vegetation NDVI dynamics and its relationship with climate, surface water and groundwater. *J Arid Environ* 113:59–68. <https://doi.org/10.1016/j.jaridenv.2014.09.010>
- Ghoraba SM (2015) Hydrological modeling of the Simly Dam watershed (Pakistan) using GIS and SWAT model. *Alex Eng J* 54:583–594. <https://doi.org/10.1016/j.aej.2015.05.018>
- Grimm NB, Grove JM, Pickett STA, Redman CL (2000) Integrated approaches to long-term studies of urban ecological systems \* the conceptual basis for studying urban ecological systems. *Bioscience* 50:571–584
- Gupta N, Mathew A, Khandelwal S (2019) Analysis of cooling effect of water bodies on land surface temperature in nearby region: a case study of Ahmedabad and Chandigarh cities in India. *Egypt J Rem Sens Space Sci* 22:81–93. <https://doi.org/10.1016/j.ejrs.2018.03.007>
- Handayani HH, Estoque RC, Murayama Y (2018) Estimation of built-up and green volume using geospatial techniques: a case study of Surabaya, Indonesia. *Sustain Cities Soc* 37:581–593. <https://doi.org/10.1016/j.scs.2017.10.017>
- Hathway EA, Sharples S (2012) The interaction of rivers and urban form in mitigating the Urban Heat Island effect: a UK case study. *Build Environ* 58:14–22. <https://doi.org/10.1016/j.buildenv.2012.06.013>
- He J, Zhao W, Li A, Wen F, Daijun Y (2019) The impact of the terrain effect on land surface temperature variation based on Landsat-8 observations in mountainous areas. *Int J Remote Sens* 40:1808–1827. <https://doi.org/10.1080/01431161.2018.1466082>
- Hua AK, Ping OW (2018) The influence of land-use/land-cover changes on land surface temperature: a case study of Kuala Lumpur metropolitan city. *Eur J Remote Sens* 51:1049–1069. <https://doi.org/10.1080/22797254.2018.1542976>
- Inamdar AK, French A, Hook S et al (2008) Land surface temperature retrieval at high spatial and temporal resolutions over the southwestern United States. *J Geophys Res Atmos* 113:1–18. <https://doi.org/10.1029/2007JD009048>
- Jahangir M, Maria Ali S, Khalid B (2016) Annual minimum temperature variations in early 21st century in Punjab, Pakistan. *J Atmos Solar-Terrestrial Phys* 137:1–9. <https://doi.org/10.1016/j.jastp.2015.10.022>
- Jamei Y, Rajagopalan P, Sun Q (2019) Spatial structure of surface urban heat island and its relationship with vegetation and built-up areas in Melbourne, Australia. *Sci Total Environ* 659:1335–1351. <https://doi.org/10.1016/j.scitotenv.2018.12.308>
- Jiménez-Muñoz JC, Sobrino JA (2009) A single-channel algorithm for land-surface temperature retrieval from ASTER data. *IEEE Geosci Remote Sens Lett* 7:176–179. <https://doi.org/10.1109/LGRS.2009.2029534>
- Jimenez-Munoz JC, Sobrino JA, Skokovic D et al (2014) Land surface temperature retrieval methods from landsat-8 thermal infrared sensor data. *IEEE Geosci Remote Sens Lett* 11:1840–1843. <https://doi.org/10.1109/LGRS.2014.2312032>
- Kothe S, Hollmann R, Pfeifroth U et al (2019) The CM SAF R Toolbox—a tool for the easy usage of satellite-based climate data in NetCDF format. *ISPRS Int J Geo-Inf* 8:109. <https://doi.org/10.3390/ijgi8030109>
- Kustas WP, Norman JM, Anderson MC, French AN (2003) Estimating subpixel surface temperatures and energy fluxes from the vegetation index-radiometric temperature relationship. *Remote Sens Environ* 85:429–440. [https://doi.org/10.1016/S0034-4257\(03\)00036-1](https://doi.org/10.1016/S0034-4257(03)00036-1)
- Latif ZA, Kamsan MES (2017) Assessing the relationship of land use land cover on surface temperature in city of Shah Alam, Malaysia using landsat-8 oli. *J Fundam Appl Sci* 9:514. <https://doi.org/10.4314/jfas.v9i5s.36>
- Li J, Song C, Cao L et al (2011) Impacts of landscape structure on surface urban heat islands: a case study of Shanghai, China. *Remote Sens Environ* 115:3249–3263. <https://doi.org/10.1016/j.rse.2011.07.008>
- Li W, Saphores JDM, Gillespie TW (2015) A comparison of the economic benefits of urban green spaces estimated with NDVI and with high-resolution land cover data. *Landsc Urban Plan* 133:105–117. <https://doi.org/10.1016/j.landurbplan.2014.09.013>
- Mallick J, Kant Y, Bharath BD (2008) Estimation of land surface temperature over Delhi using Landsat-7 ETM+. *J Ind Geophys Union* 12:131–140
- Meng X, Cheng J, Liang S (2017) Estimating land surface temperature from Feng Yun-3C/MERSI data using a new land surface emissivity scheme. *Remote Sens* 9:9–11. <https://doi.org/10.3390/rs9121247>
- Owojori A, Hongjie X (2015) Landsat image-based lulc changes of san antonio, texas using advanced atmospheric correction and object-oriented image analysis approaches. *Remote sensing image processing and analysis (ES 6973)*
- Pal S, Ziaul S (2017) Detection of land use and land cover change and land surface temperature in English Bazar urban centre. *Egypt J Remote Sens Space Sci* 20:125–145. <https://doi.org/10.1016/j.ejrs.2016.11.003>
- Peng J, Pan Y, Liu Y et al (2018) Linking ecological degradation risk to identify ecological security patterns in a rapidly urbanizing landscape. *Habitat Int* 71:110–124. <https://doi.org/10.1016/j.habitatint.2017.11.010>
- Rashid K, Rasul G (2007) Rainfall variability and maize production over the potohar plateau of Pakistan. *Pak J Meteorol* 8:63–74
- Rehman Z, Kazmi SJH, Khanum F, Samoon ZA (2015) Analysis of land surface temperature and ndvi using geo-spatial technique: a case study of Keti Bunder, Sindh, Pakistan. *J Basic Appl Sci* 11:514–527. <https://doi.org/10.6000/1927-5129.2015.11.69>
- Rong-bo X, Zhi-yun O, Hua Z et al (2007) Spatial pattern of impervious surfaces and their impacts on land surface temperature in Beijing, China. *J Environ Sci* 19:250–256
- Rosas J, Houborg R, McCabe MF (2017) Sensitivity of Landsat 8 surface temperature estimates to atmospheric profile data: a study using MODTRAN in dryland irrigated systems. *Remote Sens* 9:1–27. <https://doi.org/10.3390/rs9100988>
- Sayão VM, Demattê JAM, Bedin LG et al (2018) Satellite land surface temperature and reflectance related with soil attributes. *Geoderma* 325:125–140. <https://doi.org/10.1016/j.geoderma.2018.03.026>
- Smakhtin VU, Hughes DA (2007) Automated estimation and analyses of meteorological drought characteristics from monthly rainfall data. *Environ Model Softw* 22:880–890. <https://doi.org/10.1016/j.envsoft.2006.05.013>
- Sobrino JA, Oltra-carrió R, Sòria G et al (2012) Remote Sensing of Environment Impact of spatial resolution and satellite overpass time on evaluation of the surface urban heat island effects. *Remote Sens Environ* 117:50–56. <https://doi.org/10.1016/j.rse.2011.04.042>
- Srivani M, Hokao K, Phonekeo V (2012) Assessing the Impact of urbanization on urban thermal environment: a case study of Bangkok metropolitan. *Int J Appl Sci Technol* 2:243–256
- Suresh S, Ajay SV, Mani K (2016) Mountain landscape of Devikulam Taluk using Landsat 8 data. *Int J Res Eng Technol* 5:92–96
- Voogt JA, Oke TR (2003) Thermal remote sensing of urban climates. *Remote Sens Environ* 86:370–384. [https://doi.org/10.1016/S0034-4257\(03\)00079-8](https://doi.org/10.1016/S0034-4257(03)00079-8)
- Weng Q (2004) Thermal infrared remote sensing for urban climate and environmental studies: methods, applications, and trends. *J*

- Photogramm Remote Sens 64:335–344. <https://doi.org/10.1016/j.isprsjprs.2009.03.007>
- Weng Q, Yang S (2004) Managing the adverse thermal effects of urban development in a densely populated Chinese city. *J Environ Manag* 70:145–156. <https://doi.org/10.1016/j.jenvman.2003.11.006>
- Weng Q, Lu D, Schubring J (2004) Estimation of land surface temperature—vegetation abundance relationship for urban heat island studies. *Remote Sens Environ* 89:467–483. <https://doi.org/10.1016/j.rse.2003.11.005>
- Xiong Y, Huang S, Chen F et al (2012) The impacts of rapid urbanization on the thermal environment: a remote sensing study of Guangzhou, South China. *Remote Sens* 4:2033–2056. <https://doi.org/10.3390/rs4072033>
- Xu W, Gu S, Zhao XQ et al (2011) High positive correlation between soil temperature and NDVI from 1982 to 2006 in alpine meadow of the Three-River Source Region on the Qinghai-Tibetan Plateau. *Int J Appl Earth Obs Geoinf* 13:528–535. <https://doi.org/10.1016/j.jag.2011.02.001>
- Xu LY, Xie XD, Li S (2013) Correlation analysis of the urban heat island effect and the spatial and temporal distribution of atmospheric particulates using TM images in Beijing. *Environ Pollut* 178:102–114. <https://doi.org/10.1016/j.envpol.2013.03.006>
- Yang B, Meng F, Ke X, Ma C (2015) The impact analysis of water body landscape pattern on urban heat island: a case study of Wuhan City. *Adv Meteorol* 2015:1–7. <https://doi.org/10.1155/2015/416728>
- Zhu X, Liu D, Chen J (2012) Remote Sensing of Environment A new geostatistical approach for filling gaps in Landsat ETM+ SLC-off images. *Remote Sens Environ* 124:49–60. <https://doi.org/10.1016/j.rse.2012.04.019>

**Publisher's Note** Springer Nature remains neutral with regard to jurisdictional claims in published maps and institutional affiliations.